Contrast Sensitivity With a Subretinal Prosthesis and Implications for Efficient Delivery of Visual Information

Georges Goetz,[1,2] Richard Smith,[3] Xin Lei,[2] Ludwig Galambos,[2] Theodore Kamins,[2] Keith Mathieson,[4] Alexander Sher,[3] and Daniel Palanker[1,5]

[1]Hansen Experimental Physics Laboratory, Stanford University, Stanford, California, United States
[2]Department of Electrical Engineering, Stanford University, Stanford, California, United States
[3]Santa Cruz Institute for Particle Physics, University of California Santa Cruz, Santa Cruz, California, United States
[4]Institute of Photonics, University of Strathclyde, Glasgow, Scotland, United Kingdom
[5]Department of Ophthalmology, Stanford University, Stanford, California, United States

Correspondence: Georges Goetz, Hansen Experimental Physics Laboratory, 452 Lomita Mall, Stanford, CA 94305, USA; ggoetz@stanford.edu.

AS and DP contributed equally to the work presented here and should therefore be regarded as equivalent authors.

Submitted: June 25, 2015
Accepted: October 4, 2015

Citation: Goetz G, Smith R, Lei X, et al. Contrast sensitivity with a subretinal prosthesis and implications for efficient delivery of visual information. *Invest Ophthalmol Vis Sci*. 2015;56:7186–7194. DOI:10.1167/iovs.15-17566

Purpose. To evaluate the contrast sensitivity of a degenerate retina stimulated by a photovoltaic subretinal prosthesis, and assess the impact of low contrast sensitivity on transmission of visual information.

Methods. We measure ex vivo the full-field contrast sensitivity of healthy rat retina stimulated with white light, and the contrast sensitivity of degenerate rat retina stimulated with a subretinal prosthesis at frequencies exceeding flicker fusion (>20 Hz). Effects of eye movements on retinal ganglion cell (RGC) activity are simulated using a linear–nonlinear model of the retina.

Results. Retinal ganglion cells adapt to high frequency stimulation of constant intensity, and respond transiently to changes in illumination of the implant, exhibiting responses to ON-sets, OFF-sets, and both ON- and OFF-sets of light. The percentage of cells with an OFF response decreases with progression of the degeneration, indicating that OFF responses are likely mediated by photoreceptors. Prosthetic vision exhibits reduced contrast sensitivity and dynamic range, with 65% contrast changes required to elicit responses, as compared to the 3% (OFF) to 7% (ON) changes with visible light. The maximum number of action potentials elicited with prosthetic stimulation is at most half of its natural counterpart for the ON pathway. Our model predicts that for most visual scenes, contrast sensitivity of prosthetic vision is insufficient for triggering RGC activity by fixational eye movements.

Conclusions. Contrast sensitivity of prosthetic vision is 10 times lower than normal, and dynamic range is two times below natural. Low contrast sensitivity and lack of OFF responses hamper delivery of visual information via a subretinal prosthesis.

Keywords: retinal prosthesis, retinal degeneration, electrophysiology

Retinal degenerative diseases such as age-related macular degeneration and retinitis pigmentosa are among the most common causes of untreatable blindness in the developed world.[1] In these diseases, the image-capturing photoreceptors degrade, while cells in the image-processing layers of the retina can remain relatively intact,[2–4] albeit with sometimes extensive rewiring,[5] allowing for the possibility of sight restoration via electrical stimulation of these surviving neurons. The epiretinal approach to retinal prostheses involves direct stimulation of the retinal ganglion cells (RGCs),[6] while the subretinal approach primarily targets the bipolar cell layer.[7] With both approaches, prosthetic systems currently approved for clinical use involve cumbersome implants wired to extraocular power supplies, necessitating complex surgeries.

To address this issue, we developed a modular, easy-to-implant photovoltaic subretinal prosthesis system in which power and visual information are delivered directly to each pixel by light projected from video goggles.[7–9] The light is pulsed to provide biphasic charge-balanced stimulation[10] required for electrochemical biocompatibility. Use of a near-infrared (NIR) wavelength (880–915 nm) allows avoiding both photophobic and phototoxic effects of bright illumination. Processing of the visual signal between the camera and the head-mounted display can be individually tailored to each patient.

A recent study has demonstrated both ex and in vivo that the resolution of this implant corresponds to its 65-μm pixel pitch.[11] However, it did not address the problem of delivering multiple gray levels to the implant. In the present paper, we therefore consider retinal responses to changes in luminance over the array, comparing the full-field contrast sensitivity of prosthetic stimulation of degenerate rat retina with that of normal vision in healthy retinas. Since the contrast sensitivity with subretinal electrical stimulation was found to be much lower than normal, we explore through simulations the implications of this finding for efficient delivery of visual information.

In the case of normal vision, the statistics of natural scenes, fixational eye movements (FEMs), and the contrast sensitivity of RGCs are all well-tuned to each other and enable efficient encoding of the visual signal.[12,13] We show that the reduced contrast sensitivity and lack of OFF responses in prosthetic

vision introduces a mismatch in this encoding machinery. We predict that the majority of FEMs cannot trigger RGC responses with such low contrast sensitivity, which could explain image fading at high stimulation frequencies in patients with subretinal prostheses.[14]

Methods

Implant Fabrication

We manufactured photovoltaic arrays on silicon-on-insulator wafers using a six-mask lithographic process, as described previously.[15] To produce anodic-first pulses of electric current, we reversed the n-doped and p-doped regions in the diodes compared to the previous description. Photovoltaic arrays consisted of 70- or 140-μm pixels, separated by 5-μm trenches. Each pixel contained two photodiodes connected in series between the active and return electrodes arranged in a hexagonal array. A resistance between the active and return electrodes helps discharge them between the light pulses, thus achieving charge balance.

Electrophysiological Recordings

We obtained rats with retinal degeneration (P90–140, $n = 5$; p300–400, $n = 2$) from a Royal College of Surgeons (RCS) colony maintained at the Stanford Animal facility. Female Long-Evans adult wild type (WT) rats ($n = 4$) were purchased from Charles River (Wilmington, MA, USA). All animals were housed in a 12-hour light/12-hour dark cycle with food and water ad libitum. We conducted all experimental procedures in accordance with the Stanford University and University of California Santa Cruz institutional guidelines, and conformed to the guidelines of the Association for Research in Vision and Ophthalmology (ARVO) Statement for the Use of Animals in Ophthalmic and Vision research.

The animals were euthanized (390 mg/mL pentobarbital sodium, 50 mg/mL phenytoin sodium) before one eye was enucleated. We isolated a small piece of retina (~3 × 3-mm) and placed it on the 512-electrode recording array[16] ganglion cell side down. We recorded from one piece of retina per animal. The photovoltaic array was then placed on top of the retina, simulating a subretinal placement in vivo.[7] We ensured good contact between the retina and the stimulating and recording arrays by carefully pressing down on the implant with a plastic mesh. We perfused the retina with Ames solution (Sigma-Aldrich Corp., St. Louis, MO, USA) saturated in oxygen and kept at 27°C. Voltage waveforms were sampled and recorded at 20 kHz on each of the 512 electrodes of the recording array.[16]

Visual Stimulation

For evaluation of prosthesis-mediated vision, we activated the photovoltaic array using a NIR projection system, which consisted of a polarization-scrambled array of NIR (880 nm) laser diodes coupled into a 400-μm multimode fiber (Dilas M1F4S22-880.3-30C-SS2.1). We collimated the laser beam at the output of the fiber and used a 2° divergence microlens array diffuser to improve beam homogeneity. The beam was projected onto the implant via the camera port of an inverted microscope (Olympus IX-71, 5× objective; Olympus Corporation, Shinjiku, Tokyo, Japan). We controlled the timing, width, and amplitude of the light using a National Instruments USB-6353 data acquisition card (National Instruments, Austin, TX, USA) and custom software.

For evaluation of the natural responses to visible light, we projected the optically minified image of a 15" CRT screen (model Sony CPD-E100; Sony Corporation, Minato, Tokyo, Japan) on the photoreceptor layer of a healthy retina through the camera port of the inverted microscope. We modulated the light intensity over the full field using randomized light pulses drawn so as to keep a mean luminance level corresponding to 0.5 of the maximum brightness over the duration of the stimulus. The light flux at the 0.5 gray background level was equivalent to 19,000 photons/μm^2/s produced by a monochromatic source of wavelength 515 nm. Each intensity step lasted 0.5 seconds before a 0.5 second-long step to the following intensity (Fig. 1A). We kept intensities between the $0.5 - 0.48 = 0.02$ and $0.5 + 0.48 = 0.98$ levels, which correspond to the limits of the range of intensities over which we are able to modulate the pixels intensity on the CRT linearly. We used $n = 100$ trials for each intensity value in order to detect deviations from the spontaneous firing rate that are half its standard deviation or larger, with a P value of 0.01 and a statistical power of 0.8, for which a minimum of $n = 94$ trials is required.[17]

For evaluation of responses to prosthetic stimulation, we used a carrier waveform consisting of 20 Hz, 4-ms pulses of NIR light. We modulated the envelope of the carrier waveform using a square wave consisting of a 0.5 second-long maximum value of 2.5 mW/mm^2 (140-μm pixels) or 5 mW/mm^2 (70-μm pixels) followed by a 0.5 second-long OFF value randomly selected from a predetermined list of values between 0 and the maximum intensity (Fig. 1B). We used $n = 150$ trials for each intensity value, in order to maintain adequate statistical power with increased noise levels due to electrical stimulation.

In addition to full-field light intensity steps, we stimulated the WT retinas with a spatio-temporal white noise, which allowed us to calculate spike triggered average (STA) response of the detected RGCs.[18] Time dependence of the calculated STAs was used to classify cells into ON-center and OFF-center types.[19] The spatiotemporal monochromatic white noise stimulus consisted of 100 × 60 square pixels with each pixel 70 μm on a side, refreshed every 33.33 ms. We randomly set the relative intensity level for each pixel in each frame above or below the 0.5 mean background level at 0.5 ± 0.48. The corresponding contrast, $(I_{max} - I_{min})/(I_{max} + I_{min})$, was therefore 96%, where I_{max} and I_{min} are the maximum and minimum intensities, respectively.

Data Analysis

For prosthetic stimulation data, we initially subtracted stimulation artifacts from the raw voltage traces recorded on the electrode array and subsequently analyzed the data using custom-written software.[16] We estimated electrical stimulation artifacts by averaging their shape over many (100+) trials. The average artifact shape was subsequently aligned to the raw recordings and pointwise subtracted from them. This method was sufficient for removal of the artifact immediately following the pulse, but often insufficient for the artifact removal during the light pulse; therefore, we blanked this phase during processing of the recordings (Figs. 1C, 1D). As a consequence, all possible direct stimulation of the RGCs (latency ≤ 1 ms)[20] was ignored in our analysis.

We performed action potential detection by thresholding the artifact-removed data. All action potential waveforms were aligned to the time of maximum deflection from baseline, and we performed dimensionality reduction on the waveforms by principal component analysis, prior to expectation-maximization clustering.[16,21] For each putative neuron, we calculated the electrophysiological image (EI) of the neuron, that is, the average voltage waveform recorded on the whole multielectrode array when the neuron produced an action potential.[22–24] We discarded neurons exhibiting abnormal EIs from

Investigative Ophthalmology & Visual Science

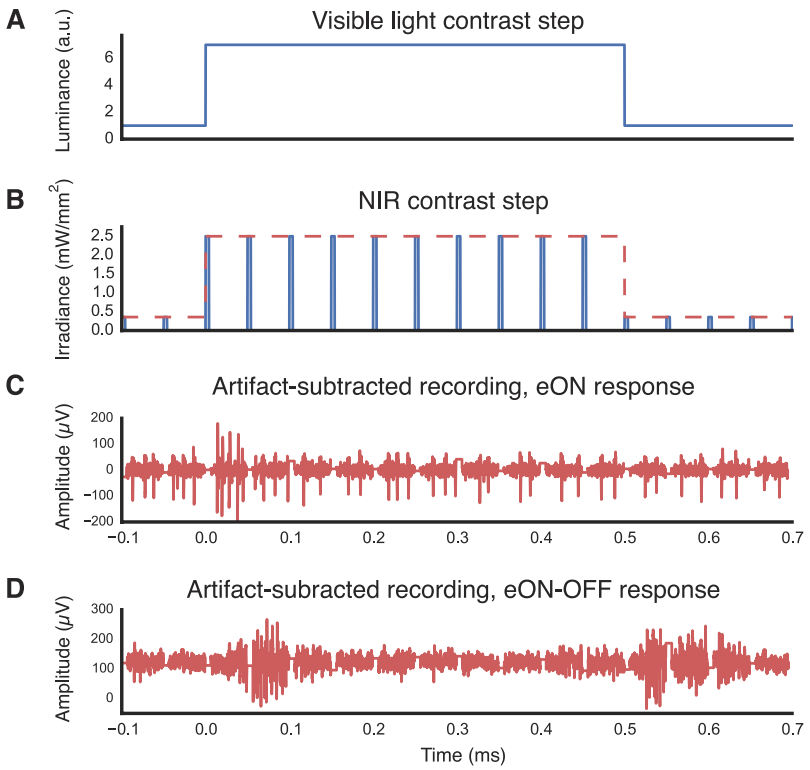

Figure 1. Stimulation protocol. (**A**) With visible illumination, contrast steps are presented using continuous illumination. (**B**) Prosthetic stimulation consists of contrast steps with the same envelope modulating a 20-Hz train of NIR pulses. (**C**, **D**) Voltage traces from two different electrodes. Note that the periodic "quiet" regions in these traces coincide with the removed stimulation artifacts during which information about the waveform was lost due to amplifier saturation. (**C**) Two neurons were detected on this electrode, one of which (larger amplitude action potentials) responded transiently to the positive contrast step while the other (smaller action potentials) did not respond to stimulation. (**D**) On this electrode, neurons transiently respond both to the positive and the negative contrast steps.

the analysis, as well as neurons for which violations of the refractory period occurred within the action potential train. Finally, we removed neurons with the same EI from the analysis, as they correspond to redundant detections of a single neuron over multiple electrodes, and only the putative neuron with the largest action potential count was kept. The neuron selection process is described in more details in the literature.[7,11]

For each contrast step, we constructed peristimulus time histograms (PSTHs) by binning action potentials over 5-ms periods and averaging over 100 (visible) or 150 (prosthesis) trials. We used the Michelson definition for contrast $(I_{post} - I_{pre})/(I_{post} + I_{pre})$, where I_{pre} is the luminance (or peak intensity for prosthetic stimulation) precontrast step and I_{post} is the luminance postcontrast step. We defined the steady-state retinal activity as the firing rate over the 300- to 500-ms period post stimulus. For visible light stimulation, we compared the steady-state activity to the activity in the 50 to 150 ms following each contrast step. The amplitude of the response was quantified as the positive variation from steady-state activity in number of action potentials. For prosthetic stimulation, latency of the elicited action potentials was shorter than for visual stimulation,[7] likely because electrical stimulation bypasses the slow phototransduction cascade. Therefore, steady-state activity was compared to the activity in the 5 to 100 ms following each contrast step. All neurons that did not respond to at least one value of contrast change with an average of 0.5 action potential elicited per trial were considered nonresponsive and were discarded from the analysis. We included in the analysis the experimental preparations in which at least 10 RGCs underneath the implant responded to 100% contrast steps over the full field.

For each neuron, we plotted the number of elicited action potentials versus amplitude of the contrast step and fitted the resulting curves with two generalized sigmoid functions, one for the OFF component of the response and the other for the ON component, such that:

$$\begin{cases} r = f(\log - c, \tau_l, \mu_l, \sigma_l, \rho_l) & \text{if } c < 0 \\ r = 0 & \text{if } c = 0 \\ r = f(\log c, \tau_l, \mu_r, \sigma_r, \rho_r) & \text{if } c > 0 \end{cases}$$

where $f(x, \tau, \mu, \sigma, \rho) = \tau(1 + e^{-(x-\mu)/\sigma})^{-\rho}$, c is the contrast and r the response of the neuron.

We defined the stimulation threshold as a 50% probability of eliciting an action potential, as estimated from the generalized sigmoid fit. We classified neurons that responded primarily to luminance increments with prosthetic stimulation as electrical ON cells, neurons that responded primarily to luminance decrements as electrical OFF cells and neurons that responded to both luminance increments and decrements as eON-OFF cells. The classification was based on three ranges of the ratio of max(ON response)/max(OFF response): $<1/3$ – eOFF, [1/3, 3] – eON-OFF and >3 – eON.

Results

RGC Responses to Contrast Steps

In normal retina, visual information is transduced by the photoreceptors, further processed in the inner nuclear layer

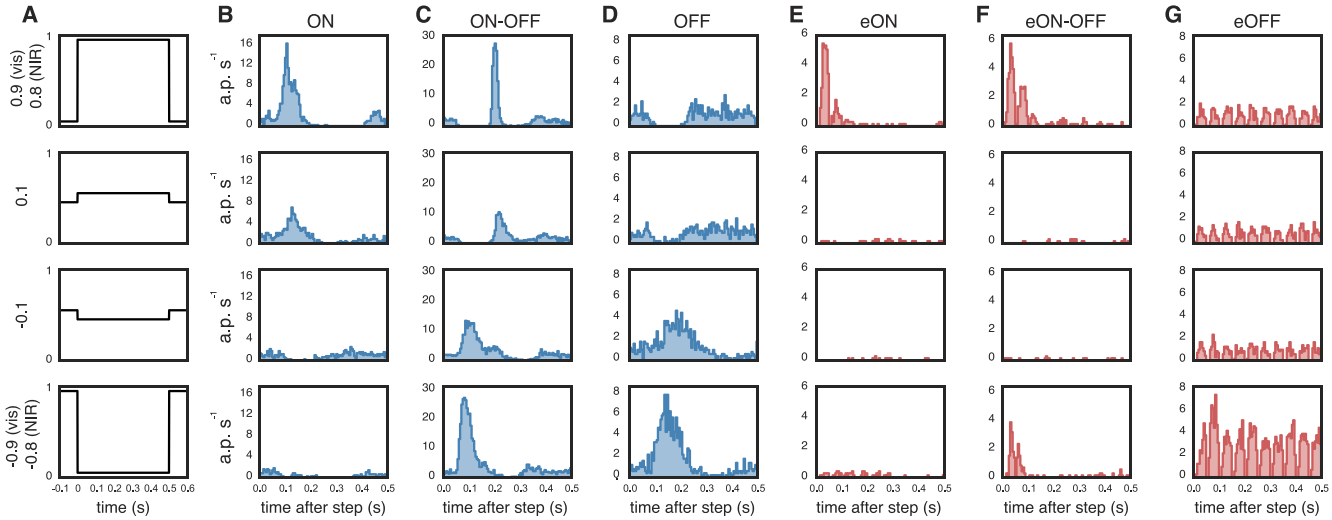

Figure 2. Single-unit responses to contrast steps. (**B**) vON, (**C**) vON-OFF, and (**D**) vOFF responses to (**A**) full-field contrast steps observed with visible light in the WT retina. Neurons responded to both high and low contrast steps. Similar (**E**) eON, (**F**) eON-OFF, and weak (**G**) eOFF responses observed with electrical stimulation in the degenerate RCS retina. With electrical stimulation, neurons did not respond to lower contrast steps. The periodic gaps in the histograms are due to electrical stimulation artifacts, which prevent detection of action potentials during the stimulation pulses.

and ultimately transmitted to the RGCs, which relay it to the brain. The receptive fields of different RGC types form complementary mosaics over the retinal surface.[19,25–28] Very generally, RGCs respond to changes in luminance by generating action potentials in response to light increments (ON-cells), or decrements (OFF-cells), or both increments and decrements in illumination (ON-OFF cells).[29] In this study, we did not classify RGCs by their direction-of-motion or object-motion selectivity.[30,31]

To measure contrast sensitivity of the healthy (WT, Long Evans) rat retina, we projected full-field visible light steps of varying amplitude on the photoreceptor layer. We projected similar patterns on a photovoltaic implant pressed on the photoreceptor side of WT and degenerate (RCS) rat retina using high frequency NIR illumination (Methods and Fig. 1). We recorded from $n = 360$ neurons for visible light stimulation of the WT retina, $n = 75$ neurons for prosthetic stimulation of the WT retina, $n = 91$ neurons for prosthetic stimulation of the P90–140 RCS retina using 70-μm pixel size implants, $n = 65$ neurons for prosthetic stimulation of the P90–140 RCS retina using 140-μm pixel size implants, and $n = 28$ neurons for prosthetic stimulation of the P300–400 RCS retina using 140-μm pixel size implants. Responses to both visible light stimulation and NIR stimulation could be classified as ON, OFF, or ON-OFF (Methods and Fig. 2). We will denote visible light responses as vON (Fig. 2B), vON-OFF (Fig. 2C), and vOFF (Fig. 2D) in the rest of the text in order to distinguish them from their prosthetic counterparts, electrical eON (Fig. 2E), eON-OFF (Fig. 2F), and rare, weak eOFF (Fig. 2G, $n = 9/75$ neurons for WT retina and $n = 2/184$ neurons for RCS retina).

Table 1. Prevalence of eON, eOFF, and eON-OFF Responses in Different Animal Models

	WT	RCS, p90–140	RCS, p300–400
eON, %	32	68	89
eON-OFF, %	56	30	7
eOFF, %	12	2	4
Cell count	75	156	28

Responses to prosthetic stimulation exhibited shorter latencies than responses to visible light (typical latency of 5–100 ms following the contrast step, as compared to latencies of 50–150 ms for visible light stimulation), likely because prosthetic stimulation bypasses the slow phototransduction cascade.[7] The ratio of prosthetic stimulation thresholds between ON-center and OFF-RGCs in WT retinas was 1.24 ± 0.31 (mean ± SEM), not substantially different between the two cell classes.

The proportion of eON, eOFF, and eON-OFF responses varied significantly between healthy and degenerate animals, as well as between RCS animals at different stages of degeneration. For WT animals, purely eON responses accounted for 32% of the responsive neurons we recorded from. For p90–140 RCS animals, this fraction went up to 68% and for p300–400 animals, 89% of the responses to electrical stimulation did not have any OFF component anymore (Table 1). In the WT retina, among OFF-center RGCs (identified from a binary white noise stimulus, Methods), 56% responded as purely eON, while 22% responded as eON-OFF and 22% as eOFF cells. ON-center RGCs responded primarily (83%) as eON-OFF cells, with another 14% responding as eON cells and the other 3% responding as eOFF cells (Table 2).

The reduction in the fraction of eOFF responses with time indicates photoreceptor involvement in their generation. Histologic analysis of the WT and RCS retina (Fig. 3) reveals that while the photoreceptor outer segments have degenerated by P90 in the RCS retina, a significant fraction of the photoreceptor somas remain, which could account for the remaining eOFF responses at P90. At P400, the photoreceptor somas are virtually all gone, as is the eOFF component of the response.

Table 2. Mapping Visible Light Responses to Prosthetic Responses

	OFF-Center	ON-Center
eON, %	56	14
eON-OFF, %	22	83
eOFF, %	22	3

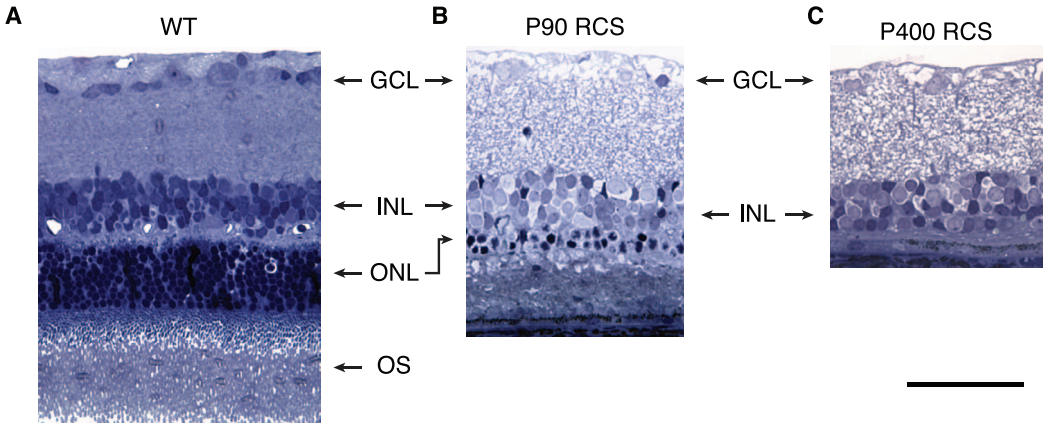

FIGURE 3. Histologic analysis of the RCS rat retina. (**A**) In the healthy WT retina, photoreceptor outer segments (OS) transduce light and modulate the membrane potential of photoreceptor somas located in the outer nuclear layer (ONL). Photoreceptors transmit neural information to cells in the inner nuclear layer (INL), which then relay it to the ganglion cells (GCL). (**B**) In the P90 RCS retina, the outer segments have been replaced by debris, and only a fraction of the photoreceptors somas remain in the INL. (**C**) At P400, all the photoreceptor somas are gone from the RCS retina and only the INL and GCL remain. *Scale bar*: 50 μm.

Contrast Sensitivity of the Retinal Response to Prosthetic Stimulation

Plotting the mean population response to contrast steps (Fig. 4) reveals two striking features of prosthetic vision, compared to natural light responses: (1) dynamic range of the responses is considerably reduced and (2) very large contrast steps are required to elicit reliable responses in the RGCs.

We defined stimulation thresholds as a 50% probability of eliciting an action potential[7,11,32,33] (Methods). For visible light stimulation, the mean stimulation threshold was 7% positive contrast for vON cells, and 3% negative contrast for vOFF cells. When stimulating p90–140 and p300–400 RCS retina with either 70-μm or 140-μm pixel size implants, stimulation threshold was measured to be between 56% (p300–400 RCS retina, 140 μm pixels) and 70% (p90–140 RCS retina, 140 μm pixels) contrast. Maximum amplitude of the response was on average 3.6 action potentials per contrast step for vON responses of the WT retina and 7.2 action potentials per contrast step for vOFF responses (Fig. 4A). Amplitude of the

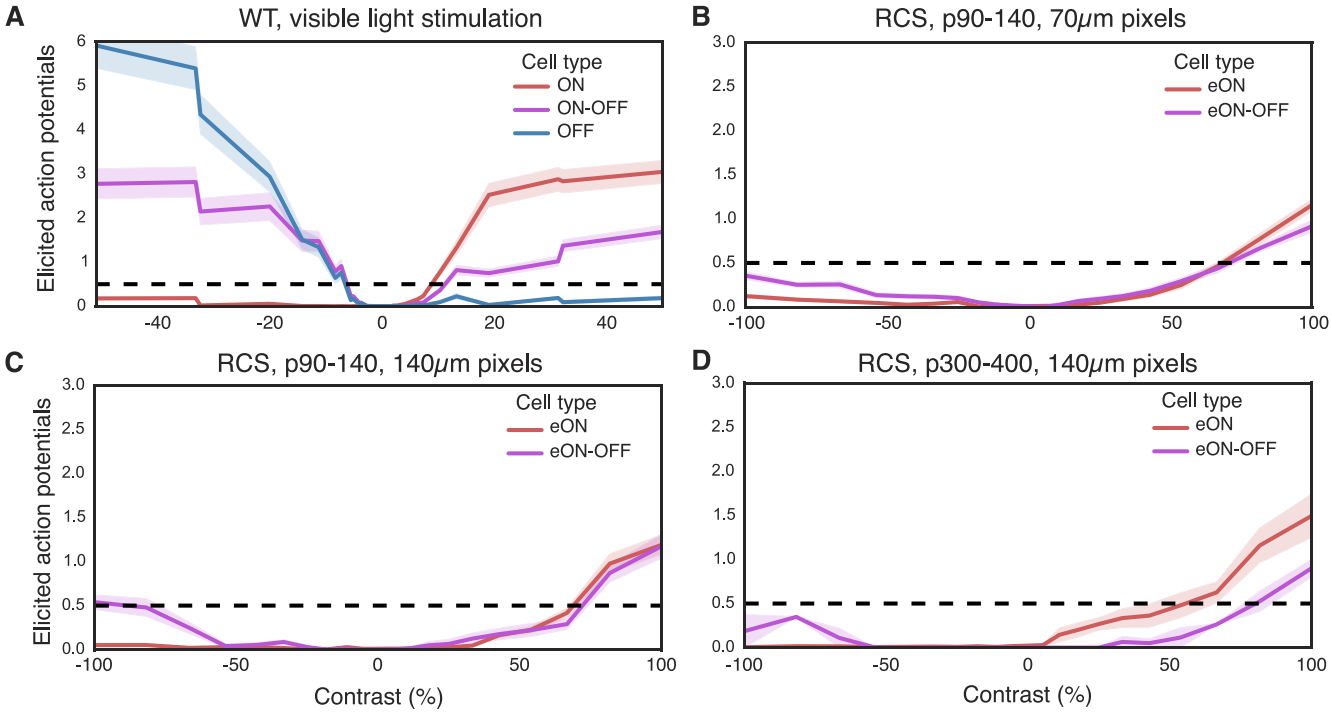

FIGURE 4. Mean population responses to contrast steps. (**A**) Wild type responses to visible full field light steps could broadly be classified into vON (*red*), vOFF (*blue*), and vON-OFF (*purple*) responses. The *black dashed line* outlines the stimulation threshold, defined as a 50% probability of eliciting an action potential correlated with the contrast step. On average, ON cells responded to contrast increments greater than 7%, while OFF cells responded to contrast decrements as small as 3%. (**B**) Photovoltaic stimulation of p90–140 RCS retina with 70-μm pixel implants requires 67% contrast steps to elicit responses in the RGCs. Maximum amplitude of the response is lower than with visible light in the WT retina. Contrast sensitivity curves are very similar with (**C**) 140-μm pixels used to stimulate p90–140 RCS retina and (**D**) in advanced stages of retinal degeneration (p300–400 RCS rats). Confidence band represents the standard error of the mean.

Investigative Ophthalmology & Visual Science

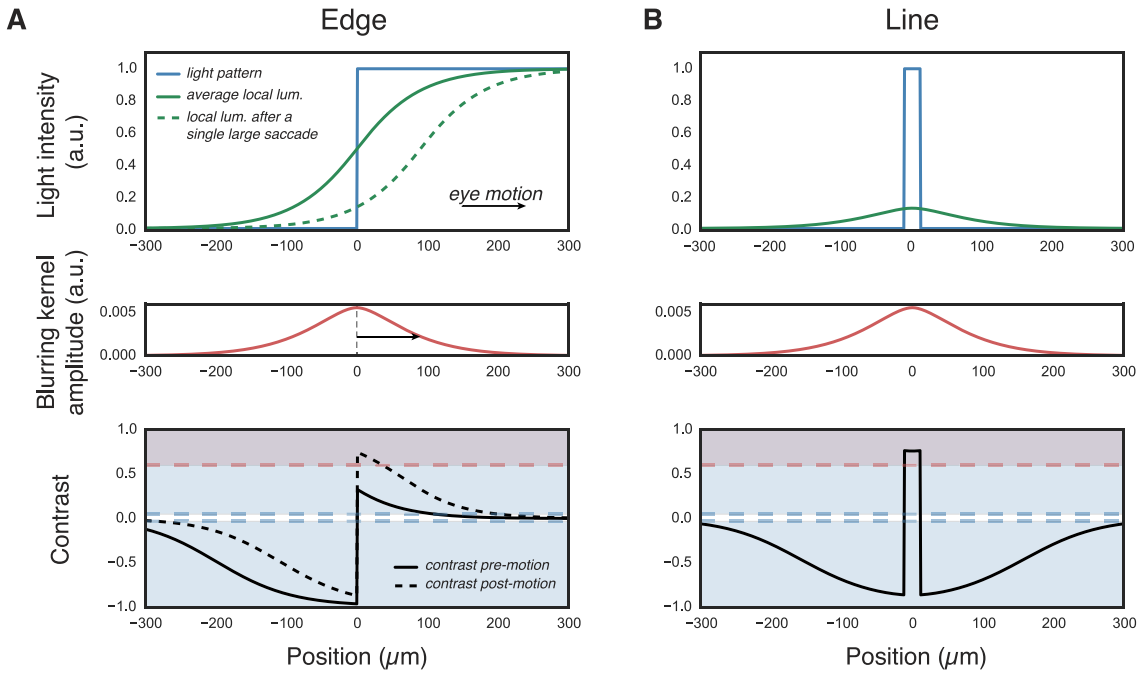

Figure 5. Effect of reduced contrast sensitivity on perception of one-dimensional patterns. The average local luminance is estimated by convolving the light pattern (*top row*) with a blurring kernel defined by the distribution of eye movements (*middle row*). The resulting local contrast is estimated and compared to full-field contrast stimulation thresholds (*bottom row*). *Red shaded area*: above threshold for prosthetic stimulation; *blue shaded area*: above threshold for visible light stimulation. (**A**) In the case of a step, the local contrast between the image and the average local luminance is below the threshold for infinitesimal eye movements (*solid green line*). Only large displacements of the visual scene will result in a sufficiently large contrast between the average local luminance and the visual scene to trigger responses (*dashed green line*, corresponding to a 90-μm lateral displacement also indicated on the blurring kernel). (**B**) In the case of a line, the pattern is sparse enough to provide contrast exceeding stimulation threshold for both natural and prosthetic vision even with small image displacements.

response was significantly reduced with prosthetic stimulation of degenerate tissue, with only 1.2 action potentials per contrast step for stimulation of p90–140 RCS, in the eON response. Since eOFF and eON-OFF responses in degenerate tissue largely disappear at the later phases of degeneration, we will ignore the few neurons that were detected as eOFF or eON-OFF in RCS tissue in further analysis.

We did not observe a significant change in contrast sensitivity thresholds or amplitude of the response of RCS retina to prosthetic stimulation with age (Figs. 4C, 4D; $P = 0.21$ and $P = 0.27$ for a change in contrast sensitivity and amplitude, respectively, 2-sample KS test), or with the size of the stimulating pixel (Figs. 4B, 4C; $P = 0.66$, 2-sample KS test): 1.2 action potentials were elicited per contrast step in p90–140 RCS retina with both 70- and 140-μm pixels, and 1.5 action potentials elicited in p300–400 RCS retina with 140-μm pixels. This result suggests that while pixel size affects stimulation thresholds,[8,34] it might not influence significantly the contrast sensitivity once the irradiance is modulated around a constant adaptation level far above stimulation threshold.

Delivering Visual Information With a Subretinal Prosthesis

Visual perception of brightness is determined primarily by local spatio-temporal contrast of the visual stimulus.[13,35,36] During visual fixation of a static scene, the retina locally adapts to the average luminance over the course of a few hundred milliseconds.[37] Retinal ganglion cells then respond to local changes in contrast triggered by ocular movements such as microsaccades, drift, and ocular tremor. It has been hypothesized that ocular movements prevent perceptual fading by continuously stimulating neurons that respond transiently to stimuli[38] and contribute to encoding of visual scenes.[13]

Fixational eye movements transform static spatial modulation in luminance in images into temporal modulation of luminance on the retina. Recent studies[12,13] have shown that the statistical properties of FEMs are well tuned to the statistics of natural scenes and perform whitening of spatial frequencies below 30 cycles per degree—the resolution limit of a typical human eye. Contrast sensitivities of RGCs are, in turn, well adapted to the resulting spatio-temporal patterns of light on the retina, producing robust RGC responses. Prosthetic vision exhibits much lower full-field contrast sensitivity and a lack of OFF responses, which is likely to disrupt these finely tuned fixational mechanisms.

To illustrate the effect of reduced contrast sensitivity on the ability of the retina to encode visual information, we considered a one-dimensional step in intensity (Fig. 5A, top panel) and estimated the contrast between the light pattern and the static component of the retinal image caused by visual fixation.[12] This static component, the local average luminance, was obtained by convolution of the light step with a blurring kernel defined by the distribution of eye movements (Fig. 5A, middle panel). The underlying assumption is that the amplitude of FEMs determines the spatial scale over which the average luminance on the retina is determined. Amplitude of the blurring kernel decreases proportionally to one minus the cumulative distribution function of microsaccades[39] and the probability distribution function of microsaccade amplitude is modeled as a gamma distribution, with shape parameter 2 and scale parameter 0.15°.

The maximum positive contrast between a step pattern and its local average luminance is 1/3, independently of the width of the blurring kernel (Fig. 5A, lower panel), much lower than

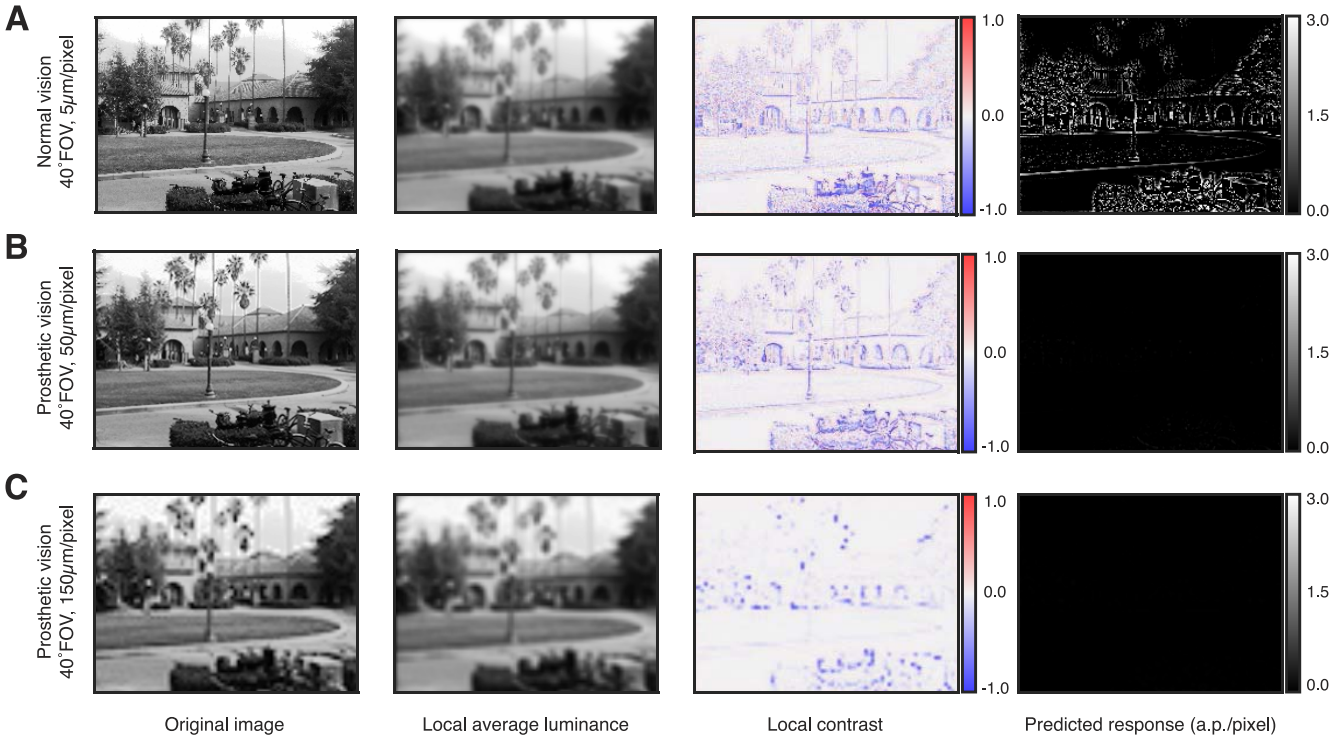

Figure 6. Prosthetic response to a natural scene. (**A**) Local contrast changes in a natural scene are large enough to elicit robust RGC responses with normal vision. With prosthetic stimulation, they are insufficient to enable image refresh through microsaccades for implants with both (**B**) 50-μm pixels and (**C**) 150-μm pixels.

the contrast stimulation threshold with prosthetic vision. Large lateral displacements of the pattern—on the order of the size of the blurring kernel—are required to cause a 60% change in local contrast. In other words, only large and rare microsaccadic eye movements can trigger a sufficient change in luminance for eliciting retinal activity.

To guarantee that any displacement of the image will trigger an ON response in a system with contrast sensitivity c, a binary image should be at least locally x-sparse, where $x = (1 - c)/(1 + c)$ on the spatial scale of the luminance averaging. In the one-dimensional case, a thin line meets this criterion (Fig. 5B), so any small displacement of the pattern can introduce sufficient changes in the local contrast to trigger a response. For prosthetic vision with contrast sensitivity thresholds around 60%, this criterion means that binary images should be at least locally 25% sparse to efficiently deliver visual information. The more images deviate from this criterion, the less retinal activity will be elicited by the temporal changes in luminance produced by FEMs.

Most static visual scenes in general, and natural scenes in particular, fail to meet such a local sparsity constraint. We exemplified this by simulating the response of prosthetic vision to natural images (Fig. 6) using a convolutional linear–nonlinear (LN) model of RGCs.[40,41] After blurring the image by convolution with the eye movement kernel (second column in Fig. 6), we calculated the contrast between the static component of the retinal image and the natural scene (Fig. 6, third column). Previously experimentally measured contrast sensitivity curves were used to convert the local contrast into RGC firing rates (Fig. 6, fourth column). With a complete characterization of the spatial dependence of contrast sensitivity of prosthetic vision, this model could be expanded to take into account the multiple spatial scales present in visual scenes and could lead to more accurate predictions.

For simulation of normal vision, we used an image with the spatial resolution of the fovea (5-μm pixel pitch on the retina, Fig. 6A). For simulation of prosthetic responses, images were first down-sampled by the pixel size in order to reflect the expected spatial resolution of the implant.[11] Therefore, we used a 50-μm and a 150-μm square lattice sampling density and contrast sensitivity curves as measured with the prosthesis (Figs. 6B, 6C). In the case of natural vision, this simple model predicts strong responses localized, as expected, around the edges and textured areas. However, in the case of prosthetic vision, it predicts almost no responses due to its poor contrast sensitivity to ON stimulation and lack of OFF responses.

Discussion

Bypassing the photoreceptors with subretinal electrical stimulation has strong implications on contrast sensitivity and dynamic range of prosthetic vision. Light stimulation of the photoreceptors leverages a finely tuned amplification cascade that can trigger responses to very dim illumination (a few photons only[42,43]), or to minute changes in contrast.[44] Prosthetic subretinal stimulation of the inner nuclear layer in the degenerate retina elicits responses with, at best, twice smaller amplitude and 10 times lower contrast sensitivity than normal.

While electrical stimulation of the healthy retina exhibits at least three types of responses to contrast steps (eON, eOFF, and eON-OFF), the eOFF component can be explained by electrical stimulation of the photoreceptor layer. If only photoreceptors, bipolar, and RGCs were involved in the response to full-field contrast steps, electrical stimulation of the photoreceptors should depolarize them, thereby triggering action potentials and therefore apparent ON response in the OFF pathway at the onset of electrical stimulation. When

electrical stimulation stops, the photoreceptors should hyperpolarize again, causing an electrical OFF response in the ON pathway this time. With full-field stimulation of the rat retina, additional amacrine cell–mediated network effects further complicate the response. This makes it difficult to pharmacologically dissect the mechanisms behind the electrical OFF response. However, its progressive and almost complete disappearance with advancing degeneration, correlated with disappearance of the photoreceptors in the RCS retina, strongly indicates that it is indeed mediated by photoreceptors.

We did not observe a difference in contrast sensitivity between implants with 70-μm and 140-μm pixels, indicative that while stimulation thresholds are affected by pixel size,[8,34] the contrast sensitivity function itself does not change once the retina adapts to above-threshold stimulation levels at high frequency (>20 Hz). The contrast sensitivity we measured matches values previously observed in vivo,[34] and, importantly, it did not decline with age of the degenerate retinas (p90–140 vs. p300–400) despite the expected changes in the retinal network.[45]

Subretinal stimulation preserves a few important features of retinal signal processing, such as flicker fusion and transient responses to slower changes in luminance, as well as nonlinear integration across subunits of RGCs with large receptive fields.[11] However, disappearance of the electrical OFF responses means that both the ON and OFF pathways are activated simultaneously, a very unnatural stimulation paradigm. Indiscriminate activation of all the cells in the inner nuclear layer is likely to contribute to reduced contrast sensitivity since both excitatory bipolar and inhibitory amacrine cells could be driven by the prosthesis. It remains unclear how this phenomenon affects phosphene perception, since current clinical trials with subretinal prosthesis demonstrated that patients see phosphenes primarily as light rather than dark flashes, and can perceive patterns of stimulation.[14]

The full-field measurements of contrast sensitivity we conducted do not take into account contrast improvements at higher spatial frequencies due to center-surround effects in normal vision.[46] It is reasonable to expect this effect to be less pronounced with a subretinal prosthesis than with normal vision since horizontal cells responsible for part of the center-surround effects in the retina are thought to only synapse directly onto photoreceptors, which disappear with degeneration, and not bipolar cells.[47] Therefore, only lateral inhibition from the amacrine cells should be able to contribute to center-surround effects with subretinal prosthetic stimulation.

Contrast sensitivity of the system with patterned stimulation[48,49] is also strongly affected by configuration of the return electrodes, and implants with distant returns exhibit significantly lower electrical contrasts as compared to implants with local returns, such as those used in this study.

Making predictions about the human visual system based on measurements with a degenerate rat retina is difficult, given the major differences between the visual systems of the two species. The midget, parasol, and small bistratified cells that dominate the human visual pathways[50] have no anatomical equivalence in rat. It is possible that the magnocellular-projecting parasol cells would have higher contrast sensitivities than the values we observed in rats. In addition, differences in the rate and extent of retinal degeneration between humans and various animal models make it even more difficult to predict responses to electrical stimulation in human patients.

An important consequence of the reduced contrast sensitivity and lack of OFF responses with prosthetic vision is that efficiency of FEMs for image refreshing and prevention of perceptual fading[13,38] is greatly diminished, compared to natural vision. While it is possible to deliver information with relatively high spatial content through the implant,[11] most static visual scenes are not sparse enough to elicit responses in RGCs with FEMs alone. This phenomenon could be responsible for the perceptual fading at high stimulation frequencies reported in patients with the subretinal implant Alpha-IMS, when FEMs that appear normal with the implant turned on[51] would be expected to trigger retinal responses. Patients prefer stimulation frequencies not exceeding 7 Hz[51,52]—well below the flicker fusion frequency, so the pulses introduce strong temporal contrast in the visual pattern. Lack of contrast sensitivity appears to be an important limitation of subretinal prosthetic devices that can strongly impede their ability to deliver visual information efficiently to the brain. This could be partially mitigated by preprocessing of the images between the camera and the implant, which by increasing local image sparsity could bring local contrast above stimulation thresholds.

Acknowledgments

We thank EJ Chichilnisky, PhD, Michael Marmor, MD, David Boinagrov, PhD, and Henri Lorach, PhD, for stimulating discussions. We are grateful to Alan Litke, PhD, Pawel Hottowy, PhD, Sergei Kachiguine, and Philip Hausser for providing access to and support of the multielectrode array recording setup. We thank Henri Lorach, Roopa Dalal, and Philip Huie for their help with histologic images.

Supported by the National Institutes of Health (Grant R01-EY-018608 [DP]), the Department of Defense (Grant W81XWH-15-1-0009 [DP]), and the Stanford Spectrum fund (DP). AS was supported by BWF CASI and Pew Charitable Trusts Scholarship in the Biomedical Sciences. KM was supported by an SU2P fellowship as part of an RCUK Science Bridges award. DP's patents related to retinal prostheses are owned by Stanford University.

Disclosure: **G. Goetz**, None; **R. Smith**, None; **X. Lei**, None; **L. Galambos**, None; **T. Kamins**, None; **K. Mathieson**, None; **A. Sher**, None; **D. Palanker**, Pixium Vision (C), P

References

1. Smith W, Assink J, Klein R, et al. Risk factors for age-related macular degeneration: pooled findings from three continents. *Ophthalmology*. 2001;108:697–704.
2. Mazzoni F, Novelli E, Strettoi E. Retinal ganglion cells survive and maintain normal dendritic morphology in a mouse model of inherited photoreceptor degeneration. *J Neurosci*. 2008;28:14282–14292.
3. Humayun MS, Prince M, de Juan E, et al. Morphometric analysis of the extramacular retina from postmortem eyes with retinitis pigmentosa. *Invest Ophthalmol Vis Sci*. 1999;40:143–148.
4. Kim SY, Sadda S, Pearlman J, et al. Morphometric analysis of the macula in eyes with disciform age-related macular degeneration. *Retina*. 2002;22:471–477.
5. Marc RE, Jones BW. Retinal remodeling in inherited photoreceptor degenerations. *Mol Neurobiol*. 2003;28:139–147.
6. Jensen RJ, Rizzo JF. Thresholds for activation of rabbit retinal ganglion cells with a subretinal electrode. *Exp Eye Res*. 2006;83:367–373.
7. Mathieson K, Loudin J, Goetz G, et al. Photovoltaic retinal prosthesis with high pixel density. *Nat Photonics*. 2012;6:391–397.
8. Mandel Y, Goetz G, Lavinsky D, et al. Cortical responses elicited by photovoltaic subretinal prostheses exhibit similarities to visually evoked potentials. *Nat Commun*. 2013;4:1980.
9. Goetz GA, Mandel Y, Manivanh R, Palanker DV, Cizmar T. Holographic display system for restoration of sight to the blind. *J Neural Engin*. 2013;10:056021.

10. Boinagrov D, Lei X, Goetz G, et al. Photovoltaic pixels for neural stimulation: circuit models and performance [published online ahead of print January 23, 2015]. *IEEE Trans Biomed Circuits Syst*. doi:10.1109/TBCAS.2014.2376528.
11. Lorach H, Goetz G, Smith R, et al. Photovoltaic restoration of sight with high visual acuity. *Nature Medicine*. 2015;21:476–482.
12. Kuang X, Poletti M, Victor JD, Rucci M. Temporal encoding of spatial information during active visual fixation. *Curr Biol*. 2012;22:510–514.
13. Rucci M, Victor JD. The unsteady eye: an information-processing stage, not a bug. *Trends Neurosci*. 2015;38:195–206.
14. Stingl K, Bartz-Schmidt K-U, Gekeler F, Kusnyerik A, Sachs H, Zrenner E. Functional outcome in subretinal electronic implants depends on foveal eccentricity. *Invest Ophthalmol Vis Sci*. 2013;54:7658–7665.
15. Wang L, Mathieson K, Kamins TI, et al. Photovoltaic retinal prosthesis: implant fabrication and performance. *J Neural Engin*. 2012;9:046014.
16. Litke AM, Bezayiff N, Chichilnisky EJ, et al. What does the eye tell the brain? Development of a system for the large-scale recording of retinal output activity. *IEEE Trans Nuclear Sci*. 2004;51:1434–1440.
17. Whitley E, Ball J. Statistics review 4: sample size calculations. *Crit Care*. 2002;6:335–341.
18. Chichilnisky EJ. A simple white noise analysis of neuronal light responses. *Network*. 2001;12:199–213.
19. Chichilnisky EJ, Kalmar RS. Functional asymmetries in ON and OFF ganglion cells of primate retina. *J Neurosci*. 2002;22:2737–2747.
20. Boinagrov D, Pangratz-Fuehrer S, Goetz G, Palanker D. Selectivity of direct and network-mediated stimulation of the retinal ganglion cells with epi-, sub- and intra-retinal electrodes. *J Neural Engin*. 2014;11:026008.
21. Lewicki MS. A review of methods for spike sorting: the detection and classification of neural action potentials. *Network*. 1998;9:R53–R78.
22. Petrusca D, Grivich MI, Sher A, et al. Identification and characterization of a Y-like primate retinal ganglion cell type. *J Neurosci*. 2007;27:11019–11027.
23. Greschner M, Field GD, Li PH, et al. A polyaxonal amacrine cell population in the primate retina. *J Neurosci*. 2014;34:3597–3606.
24. Li PH, Gauthier JL, Schiff ML, et al. Anatomical identification of extracellularly recorded cells in large-scale multielectrode recordings. *J Neurosci*. 2015;31:4663–4675.
25. Devries SH, Baylor DA. Mosaic arrangement of ganglion cell receptive fields in rabbit retina. *J Neurophysiol*. 1997;78:2048–2060.
26. Field GD, Sher A, Gauthier JL, et al. Spatial properties and functional organization of small bistratified ganglion cells in primate retina. *J Neurosci*. 2007;27:13261–13272.
27. Dacey DM, Petersen MR. Dendritic field size and morphology of midget and parasol cells of the human retina. *PNAS*. 1992;89:9666–9670.
28. Wassle H. Parallel processing in the mammalian retina. *Nat Rev Neurosci*. 2004;5:747–757.
29. Heine WF, Passaglia CL. Spatial receptive field properties of rat retinal ganglion cells. *Vis Neurosci*. 2011;28:403–417.
30. Borst A, Euler T. Seeing things in motion: models, circuits, and mechanisms. *Neuron*. 2011;71:974–994.
31. Olveczky BP, Baccus S, Meister M. Segregation of object and background motion in the retina. *Nature*. 2003;423:401–408.
32. Sekirnjak C, Hottowy P, Sher A, Dabrowski W, Litke AM, Chichilnisky EJ. Electrical stimulation of mammalian retinal ganglion cells with multielectrode arrays. *J Neurophysiol*. 2006;95:3311–3327.
33. Jepson LH, Hottowy P, Mathieson K, et al. Focal electrical stimulation of major ganglion cell types in the primate retina for the design of visual prostheses. *J Neurosci*. 2013;33:7194–7205.
34. Lorach H, Goetz G, Mandel Y, et al. Performance of photovoltaic arrays in-vivo and characteristics of prosthetic vision in animals with retinal degeneration. *Vision Res*. 2015;111(pt B):142–148.
35. Shapley RM, Enroth-Cugell C. Visual adaptation and retinal gain controls. In: Osborne N, Chader G, eds. *Progress in Retinal Research*. Pergamon Press: Oxford; 1984:263–346.
36. Shapley RM, Kaplan E, Purpura KP. Contrast sensitivity and light adaptation in photoreceptors or in the retinal network. In: Shapley RM, Lam DM-K, eds. *Contrast Sensitivity*. MIT Press: Cambridge, MA; 1993:103–116.
37. Shapley RM. Retinal physiology: adapting to the changing scene. *Curr Biol*. 1997;7:R412–R423.
38. McCamy MB, Otero-Millan J, Macknik SL, et al. Microsaccadic efficacy and contribution to foveal and peripheral vision. *J Neurosci*. 2012;32:9194–9204.
39. Martinez-Conde S, Macknik SL, Troncoso XG, Hubel DH. Microsaccades: a neurophysiological analysis. *Trends Neurosci*. 2009;32:463–475.
40. Paninski L. Maximum likelihood estimation of cascade point-process neural encoding models. *Network*. 2004;15:243–262.
41. Truccolo W, Eden UT, Fellows MR, Donoghue JP, Brown EN. A point process framework for relating neural spiking activity to spiking history, neural ensemble, and extrinsic covariate effects. *J Neurophysiol*. 2005;93:1074–1089.
42. Baylor DA, Lamb TD, Yau K-W. The membrane current of single rod outer segments. *J Physiol*. 1979;288:589–611.
43. Rieke F, Baylor DA. Single-photon detection by rod cells of the retina. *Rev Modern Phys*. 1998;70:1027–1036.
44. van Alphen B, Winkelman BH, Frens MA. Age- and sex-related differences in contrast sensitivity in C57BL/6 mice. *Invest Ophthalmol Vis Sci*. 2009;50:2451–2458.
45. Marc RE, Jones BW, Watt CB, Strettoi E. Neural remodeling in retinal degeneration. *Prog Retin Eye Res*. 2003;22:607–655.
46. Derrington AM, Lennie P. Spatial and temporal contrast sensitivities of neurones in lateral geniculate nucleus of macaque. *J Physiol*. 1984;357:219–240.
47. Kolb H, Mariani A, Gallego A. A second type of horizontal cell in the monkey retina. *J Comp Neurol*. 1980;189:31–44.
48. Palanker D, Vankov A, Huie P, Baccus S. Design of a high-resolution optoelectronic retinal prosthesis. *J Neural Eng*. 2005;2:S105–S120.
49. Loudin JD, Simanovskii DM, Vijayraghavan K, et al. Optoelectronic retinal prosthesis: system design and performance. *J Neural Eng*. 2007;4:S72–S84.
50. Dacey DM. Origins of perception: retinal ganglion cell diversity and the creation of parallel visual pathways. In: Gazzaniga MS, ed. *The Cognitive Neurosciences*. MIT Press: Cambridge, MA; 2004:281–301.
51. Hafed ZM, Stingl K, Bartz-Schmidt KU, Gekeler F, Zrenner E. Oculomotor behavior of blind patients seeing with a subretinal visual implant [published online ahead of print April 20, 2015]. *Vision Res*. doi:10.1016/j.visres.2015.04.006.
52. Stingl K, Bartz-Schmidt KU, Besch D, et al. Artificial vision with wirelessly powered subretinal electronic implant alpha-IMS. *Proc Biol Soc*. 2013;280:20130077.